Effect of pore size distribution on iron oxide coated granular activated carbons for phosphate adsorption – Importance of mesopores

Suresh Kumar, Prashanth; Prot, Thomas; Korving, Leon; Keesman, Karel J.; Dugulan, A.I.; van Loosdrecht, Mark C.M.; Witkamp, Geert Jan

DOI
10.1016/j.cej.2017.05.147

Publication date
2017

Document Version
Final published version

Published in
Chemical Engineering Journal

Citation (APA)
Suresh Kumar, P., Prot, T., Korving, L., Keesman, K. J., Dugulan, A. I., van Loosdrecht, M. C. M., & Witkamp, G. J. (2017). Effect of pore size distribution on iron oxide coated granular activated carbons for phosphate adsorption – Importance of mesopores. *Chemical Engineering Journal*, *326*, 231-239. https://doi.org/10.1016/j.cej.2017.05.147

Chemical Engineering Journal 326 (2017) 231–239

Contents lists available at ScienceDirect

Chemical Engineering Journal

journal homepage: www.elsevier.com/locate/cej

Effect of pore size distribution on iron oxide coated granular activated carbons for phosphate adsorption – Importance of mesopores

Prashanth Suresh Kumar [a,b], Thomas Prot [a], Leon Korving [a], Karel J. Keesman [a,c], Iulian Dugulan [d], Mark C.M. van Loosdrecht [b], Geert-Jan Witkamp [b,*]

[a] Wetsus, European Centre of Excellence for Sustainable Water Technology, Oostergoweg 9, 8911 MA Leeuwarden, The Netherlands
[b] Dept. Biotechnology, Applied Sciences, Delft University of Technology, Building 58, Van der Maasweg 9, 2629 HZ Delft, The Netherlands
[c] Biobased Chemistry and Technology, Wageningen University, Bornse Weilanden 9, 6708 WG Wageningen, The Netherlands
[d] Fundamental Aspects of Materials and Energy Group, Delft University of Technology, Mekelweg 15 JB, Delft, The Netherlands

HIGHLIGHTS

- Phosphate adsorption affinity is proportional to the mesoporous area of the adsorbents.
- Ferrihydrite nanoparticles are formed on GAC using $KMnO_4$.
- Iron oxide coating is not evident in the micropores of GAC.
- Manganese loading is an important intermediary step in coating iron oxide.

GRAPHICAL ABSTRACT

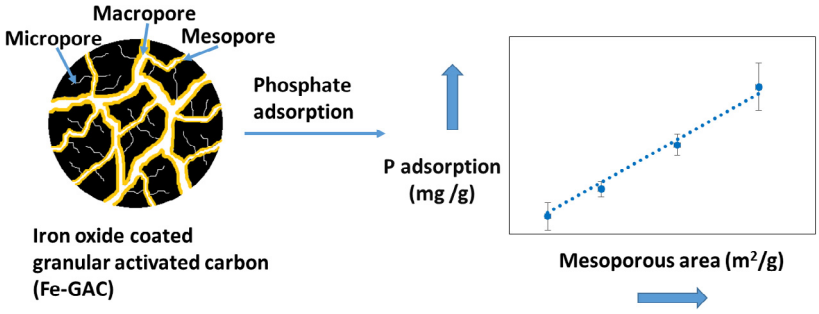

ARTICLE INFO

Article history:
Received 17 May 2017
Accepted 24 May 2017
Available online 26 May 2017

Keywords:
Adsorption affinity
Iron coating
Non Local Density Functional Theory (NLDFT)
Mesopores
Oxidized activated carbon

ABSTRACT

Adsorption is often suggested for to reach very low phosphate levels in municipal wastewater effluent and even to recover phosphate. Adsorbent performance is usually associated with surface area but the exact role of the pore size distribution (PSD) is unclear. Here, we show the effect of the PSD on phosphate adsorption. Granular activated carbons (GACs) with varying PSDs were treated with potassium permanganate followed by reaction with ferric chloride to form iron oxide coated GACs (Fe-GACs). Energy dispersive X-ray and kinetics experiments confirmed that manganese anchored on the GAC is important for subsequent iron attachment. Mössbauer spectroscopy showed presence of ferrihydrite in Fe-GAC. Transmission electron microscopy showed that the iron oxide particles are not present in the micropores of the GACs. Phosphate adsorption isotherms were performed with the Fe-GACs and adsorption at lower phosphate concentrations correlated with the porous area of >3 nm of the adsorbents, a high fraction of which is contributed by mesopores. These results show that high surface areas of GACs resulting from micropores do not contribute to adsorption at low phosphate concentrations. This can be explained by the micropores being difficult to coat with iron oxide nanoparticles, but in addition the diffusion of phosphate into these pores could also be hindered. It is therefore recommended to use backbones having high mesoporous areas. This information is useful for developing adsorbents particularly for applications treating low phosphate concentrations, for e.g. in municipal wastewater effluent polishing.

1. Introduction

Phosphorus is an essential nutrient for life. Humans consume phosphorus via food and the excreted phosphorus ends up as

* Corresponding author.
E-mail address: G.J.Witkamp@tudelft.nl (G.-J. Witkamp).

http://dx.doi.org/10.1016/j.cej.2017.05.147
1385-8947/

phosphate in municipal wastewater treatment plants [1,2]. In water bodies such as lakes and rivers, the presence of excess dissolved phosphate, especially as inorganic orthophosphate (we refer to this as phosphate henceforth), leads to algal bloom/eutrophication [3]. This affects the water quality and hence the ecosystem. Adsorption is often suggested as an effluent polishing step to keep the phosphate discharge from municipal wastewater treatment plants down to very low concentrations [4,5]. Iron (hydr)oxides have regularly been used as phosphate adsorbents due to their good binding capacity with phosphate [6,7]. In order to facilitate recovery of adsorbent particles, increase their stability and enhance the surface area (and hence the adsorption), adsorbents are coated onto granular materials [5,8,9]. One such backbone on to which iron oxide can be coated is granular activated carbon (GAC). Activated carbon is becoming an essential component in water treatment facilities due to its ability to adsorb several contaminants from water. This includes micropollutants, organic compounds, odour and color removal [10–12]. Activated carbon has a huge surface area, is relatively cheap, and in the form of granules (GAC) it offers the possibility for regeneration and reuse [10]. The need for increasing affinity of activated carbon towards specific contaminants has led to studies on its surface modification [13]. It is coated with different metal oxides, including iron oxides, to improve specific interaction with phosphate [9,14–16].

A key parameter for gauging the performance of an adsorbent is its adsorption capacity. Table S1 in Supporting information compares adsorption capacity of different iron oxide based adsorbents from literature. Normally adsorbent capacities are expressed in terms of mass of the total adsorbent. However when the adsorption capacity is expressed in terms of the iron present some adsorbents loaded with iron oxide show very high specific adsorption capacities. For instance, an earlier study [9] on GAC coated with magnetite (Fe_3O_4), showed a very high maximum adsorption capacity of 141.8 mg P/g Fe indicating the iron oxide (magnetite) was formed as nanoparticles or as a thin layer which is accessible to phosphate. However, a calculation shows that even if monolayer coverage of the iron particles is assumed, less than 10 m^2/g can be covered with iron oxide ((text S1(c)), whereas typically 700–1600 m^2/g is available in GAC's (Tables S1 and S3).

This suggests that optimization of the iron distribution may lead to a significantly improved capacity of phosphate adsorption in these adsorbents and this was the objective of our study. To achieve this we focused on two important aspects. Firstly, we studied the mechanism of coating iron oxide on GAC. Secondly, we evaluated the effect of pore size distribution (PSD) of the GAC in relation to coating iron oxide and adsorbing phosphate. While trying to improve adsorbents, the main focus is usually their surface area and not much attention is given to their PSD. The PSD may however be very important for a good distribution of these nanoparticles, because based on the size of the nanoparticles, not all pores might be available for coating. Also the pore size could influence the rate of diffusion of the phosphate molecules into the adsorbent. To the best of our knowledge, there are no earlier studies focusing on the effect of PSD of GAC based adsorbents in phosphate adsorption. Our study provides an insight on this aspect and explains how PSD could be key to improving iron based adsorbents for phosphate adsorption.

2. Experimental

2.1. Chemicals

Five different GACs were evaluated in the study and designated as GAC-1, 2, 3, 4 and 5 (Table S3 in Supporting information lists their general characteristics). GAC-1 and GAC-2 were obtained from the activated carbon suppliers Norit and Desotech respectively. GAC-3, 4 and 5 were obtained from Mast Carbons (UK). Hydrogen peroxide (H_2O_2), nitric acid (HNO_3), potassium dihydrogen phosphate (KH_2PO_4), and potassium permanganate ($KMnO_4$) were obtained from VWR chemicals. Ferric chloride hexahydrate ($FeCl_3{\cdot}6H_2O$), hypochloric acid ($HClO_4$) were obtained from Sigma Aldrich, Boom BV (Netherlands), respectively. Manganese (IV) oxide (MnO_2) and nitric acid (HNO_3) were obtained from Merck. Iron color disc test kit (Range: 0–5 mg Fe/L) was obtained from Hach.

2.2. Characterizing surface area and PSD

About 0.1 g of dried samples were degassed overnight in the presence of nitrogen gas. Subsequently nitrogen adsorption and desorption cycles were carried out using Micromeritics TriStar 3000. The data from the nitrogen adsorption-desorption profiles were fitted with models included in the analysis software to obtain the Brunauer-Emmett-Teller (BET) surface and Barret-Joyner-Halenda (BJH) PSD, and the pore area and PSD from Non Local Density Functional Theory (NLDFT).

2.3. Evaluating mechanism of iron oxide formation on GAC

The iron oxide coating on the GAC was done in two successive steps: first a reaction with an oxidizing agent then followed by reacting with ferric chloride solution. In between each step, the GAC was thoroughly washed with distilled water and oven dried (105 °C). The GACs treated with $KMnO_4$ were washed till the washed solution turned from pink to colorless. After reacting with ferric chloride, the washing of the GAC was carried out until the iron content of the washed solution reached below the detection limit (0.2 mg Fe/L) when measured by iron color disc test kit. Unless otherwise mentioned, the solid to liquid ratio was 1 g GAC for 10 ml of solution, and all the reactions were allowed to proceed overnight (~18 h) and at room temperature (22 °C).

2.3.1. Effect of different oxidizing agents

Initially, 5 g of GAC-1 was reacted with 5 M aqueous solutions of either H_2O_2, $HClO_4$, HNO_3, or with 0.4 M $KMnO_4$. Subsequently, 3 g of the oxidized GAC-1 was reacted with 20 g Fe/L ferric chloride solution. The resulting iron oxide coated GACs are called Fe-GACs. The Fe-GACs were cross-sectioned and a surface elemental analysis was done at an acceleration voltage of 15 kV using Oxford Instruments x-act SDD Energy Dispersive X-ray Spectrometer (EDX).

2.3.2. Role of manganese in iron loading

For profiling the distribution of iron in relation to manganese, 5 g of GAC-1 was mixed with 200 ml of 0.4 M $KMnO_4$ in separate beakers for 15 min, 2 h and 24 h respectively. Three granules from each batch (after washing and drying) were analyzed for manganese distribution on their cross-section using EDX. The imaging was done using a JEOL JSM-6480 LV Scanning Electron Microscope (SEM). The change in mass of total granules as a result of taking 3 granules from each batch was negligible. The remaining granules from each batch were reacted in three separate beakers with 50 ml of 20 g Fe/L ferric chloride solution for 24 h. Preliminary experiments showed that iron loading equilibrium was reached within this timeframe. The GAC-1 from the different beakers was washed, oven dried and their cross-sections were analyzed for iron distribution using EDX.

For evaluating the anchorage of iron as a function of manganese released, 5 g of GAC-3 was reacted with a 0.2 M $KMnO_4$ solution and subsequently 3 g of oxidized GAC-3 was treated with 20 g Fe/L solution. 0.1 g of granules were sampled at different intervals of time (10, 30, 60, 120, 240, 375 min and 27 h). These samples

were microwave digested using 67% HNO_3. The iron and manganese concentrations in the digested solution was measured using a Perkin Elmer Optima 5300 DV Inductively Coupled Plasma Optical Emission Spectroscopy (ICP-OES). As will be explained in the discussion section, the anchorage of iron on manganese was evaluated by replicating the same conditions but in the absence of GAC. To determine this, 710 mg of MnO_2 was added to 50 ml of 20 g Fe/L, and the solution was monitored for iron and manganese concentrations at 15, 30, 60, 180, 360 min and 24 h.

2.3.3. Characterization of Fe-GAC

Fe-GAC based on GAC-3 (which had been produced by treating with 50 ml of 0.4 M $KMnO_4$) was dried and grinded. This sample was analyzed using Mössbauer spectroscopy to determine the type of iron oxide. Transmission ^{57}Fe Mössbauer spectra were collected at different temperatures with conventional constant acceleration and sinusoidal velocity spectrometers using a ^{57}Co (Rh) source. Velocity calibration was carried out using an α-Fe foil. The Mössbauer spectra were fitted using the Mosswin 4.0 program [17]. GAC-3, GAC-3 oxidized with $KMnO_4$ (having highest manganese loading), and Fe-GAC from GAC-3 (having highest iron loading) were examined with JEOL JEM 1400 Transmission Electron Microscope (TEM). The GAC-3 oxidized with $KMnO_4$ and corresponding Fe-GAC were also evaluated by X-ray diffraction measurements (XRD). The XRD measurements were carried out using a PANalytical X'Pert pro X-ray diffractometer mounted in the Bragg-Brentano configuration with a Cu anode (0.4 mm × 12 mm line focus, 45 kV, 40 mA). The X-ray scattered intensities were measured with a real time multi strip (RTMS) detector (X'Celerator). The data were collected in the angle range $5° < 2\theta < 90°$ with a step size of 0.008° (2θ); total measuring time was 1 h.

2.4. Manganese and iron loading on GACs with different PSD

Fe-GACs were produced from GAC-1, 2, 3, 4 and 5 by reacting them with varying amounts of $KMnO_4$. Since $KMnO_4$ is close to its solubility limit at 0.4 M, the amount of $KMnO_4$ available for the GACs was varied by a combination of adjusting the concentration and the solution volume. For GAC-1, 2, 4 and 5, 5 g of GAC was reacted with 25 ml of 0.08, 0.2, 0.4, and with 50 ml, 100 ml and 200 ml of 0.4 M $KMnO_4$. GAC-3 had a low density and 5 g could not be completely submerged in 25 ml solutions. So these solutions were instead replaced with 50 ml of 0.04, 0.1, and 0.2 M $KMnO_4$, so that the amount of $KMnO_4$ exposed per gram of GAC was constant for all GAC's.

2.5. Phosphate adsorption

For evaluating adsorption kinetics, Fe-GACs from GAC-1, 2 and 3, i.e. Fe-GAC-1, Fe-GAC-2, Fe-GAC-3, were added to 100 ml of 20 mg P/L at different intervals of time (5, 15, 30, 60, 90, 120, 180, 360 min, 24, 48, 72 and 96 h). For determining the adsorption isotherms, Fe-GAC-1, Fe-GAC-2 and Fe-GAC-3 were added to 100 ml aqueous solutions with phosphate concentrations of 1, 5, 10, 25, 50, 75 and 100 mg P/L and the experiment was run for 96 h. For the adsorption kinetics as well the isotherms, the adsorbent concentration was 2 g/L, with solution pH of 6.5 and at room temperature (22 °C). For Fe-GAC-1 and Fe-GAC-2 the samples with highest iron loading was used. However, for Fe-GAC-3, the sample with highest iron loading had become powdered. Hence, for Fe-GAC-3, the sample produced by treating with 50 ml of 0.4 M $KMnO_4$ was used, as this was still granular. To check adsorption of phosphate on $KMnO_4$ treated GAC, the GAC-3 treated with 100 ml of 0.4 M $KMnO_4$ was also tested at the same adsorbent dose and a phosphate concentration of 100 mg P/L. The phosphate concentration in solutions was measured using Metrohm 761 compact Ion Chromatograph (IC).

2.6. Data fitting and error determination

All the experiments were run as duplicates and the average value was reported with the standard deviation, unless otherwise indicated. For adsorption kinetics and isotherms, model parameters were fitted by a non-linear regression approach as per Microsoft Excel's Solver program. For determining the errors in fitted model parameters, the standard deviations of the parameter estimates ($\hat{\theta}$) were calculated from the covariance matrix. Here, the 2 × 2 covariance matrix is calculated as follows:

$$Cov(\hat{\theta}) = \frac{\varepsilon(\hat{\theta})^T \varepsilon(\hat{\theta})}{n-p}\left(X(\hat{\theta})^T X(\hat{\theta})\right)^{-1} \quad (1)$$

where, n denotes the number of samples, p denotes the number of parameters, $\varepsilon(\hat{\theta})$ denotes the error vector between the experimental and corresponding model output values, and $X(\hat{\theta})$ is the sensitivity matrix, which consists of the partial derivatives of the model output as a function of the estimated parameters.

The standard deviations of the parameter estimates are calculated by taking the square root of the diagonal of the covariance matrix [18]. A more elaborate description on determining the sensitivity matrix is provided under text S2 in Supporting information.

3. Results and discussion

3.1. Characterizing the PSD of different GACs

As per International Union of Pure and Applied Chemistry (IUPAC), porous materials can be classified into three categories based on the pore diameters. These are macropores (>50 nm), mesopores (2–50 nm), and micropores (<2 nm) [19,20]. The PSD of porous materials can be determined by gas adsorption and desorption profiles [21], for example by a nitrogen adsorption analyzer. The gas adsorption and desorption profiles can be fit with models (inbuilt in the software) to obtain information on the specific surface area, porosity and PSD of the materials. These include classical, macroscopic models like BJH (Barret-Joyner-Halenda) [22], or models like NLDFT (Non Local Density Functional Theory) which connect macroscopic properties to the behavior at molecular scale [23]. The main differences between these models are the underlying assumptions regarding the mechanism of pore filling. BJH models assume that pore filling via pore condensation results in well-defined interfaces in the pores. This assumption works for macropores and large mesopores, but fails to accurately describe micropores and small mesopores [23]. The NLDFT model considers the difference in thermodynamic properties of a fluid confined in a pore as opposed to bulk fluid, and is able to give a more accurate description of micropores and mesopores [24]. The NLDFT model is widely used for characterizing materials like activated carbon, which consist of a high fraction of micropores [25]. For the purpose of our study, we want to characterize the whole PSD (micro, meso and macropores) of the GACs and hence we evaluate the GACs using both the BJH and NLDFT models as shown in Fig. 1. The PSD is also shown in terms of pore area instead of pore volume in Fig. S1 in Supporting information. It should be noted that the values obtained from the model are originally provided as a function of pore diameter intervals (graphs of incremental volume will be histograms) which are not equal. The plots are plotted in terms of average diameter (as is often done) for the clarity of the readers.

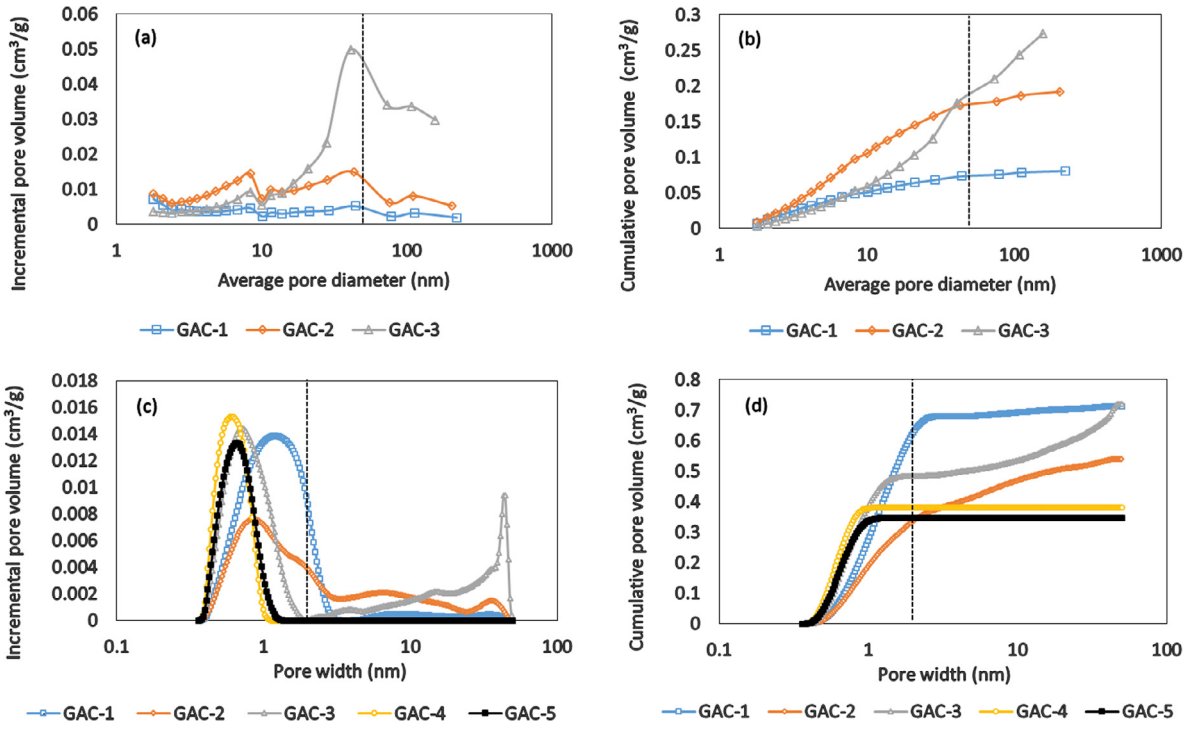

Fig. 1. Incremental PSD of different GACs using (a) BJH model, (c) NLDFT model. Cumulative PSDs of different GACs using (b) BJH model, (d) NLDFT model. The dashed lines within BJH model plots (a & b) show cut off between meso and macropores (50 nm). The dashed lines within NLDFT model plots (c & d) show cut off between micro and mesopores (2 nm).

Fig. 1(a and b) shows that the GACs have a higher fraction of macroporous volume in the following order: GAC-3 > GAC-2 > GAC-1. GAC-4 and GAC-5 were very microporous and hence could not be fitted by the BJH model. Fig. 1(c & d) confirms using the NLDFT model that GAC-4 and GAC-5 are completely microporous. The other GACs have a higher fraction of mesoporous volume in the following order: GAC-3 > GAC-2 > GAC-1. For all the GACs, more than 90% of the total pore area is contributed by micropores (Table S4 in Supporting information).

Fig. 1 demonstrates that the different GACs have indeed different PSDs. This information is relevant for later discussions where we highlight the importance of PSD for coating iron oxides onto GAC and subsequently for phosphate adsorption. Other information on the different GACs like BET surface area, particle size and shape are provided in Table S3 in Supporting information.

3.2. Mechanism of coating iron oxide on GAC

3.2.1. Iron loading on GAC using different oxidizing agents

Amongst the different methods used for surface modification of activated carbon, the use of oxidizing agents is the most common method [13]. We used the same approach for coating of our GACs with iron oxide. Activated carbon has previously been coated with iron oxide by using nitric acid [26]. The hypothesis is that surface oxidation of GAC introduces oxidized functional groups to which the dissolved iron reacts to form iron oxides [26]. We used four commonly used oxidizing agents for surface modification of GAC, namely: H_2O_2, $HClO_4$, HNO_3 and $KMnO_4$. Fig. 2 describes the effect of the different oxidizing agents on iron loading on GAC-1.

Fig. 2(a) shows that $KMnO_4$ resulted in maximum iron loading (54 mg Fe/g GAC). This was 7 times better than the next best oxidizer used (HNO_3). Fig. 2(b) shows the iron to oxygen molar ratio on the GACs as determined by EDX (Table S2 in Supporting information shows the oxygen and iron content for the different samples). Although EDX gives a semi quantitative estimate of the

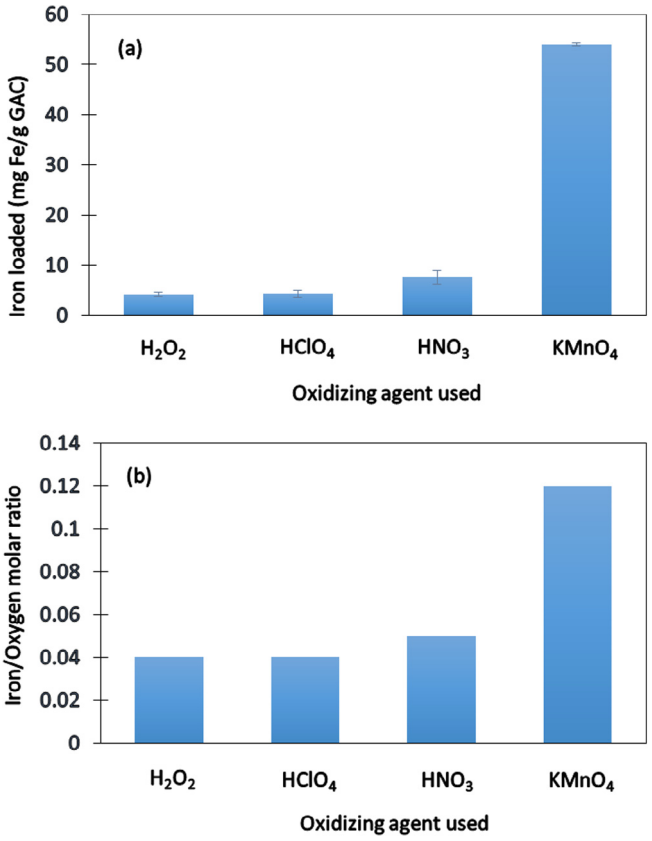

Fig. 2. (a) Iron loading on GAC-1 via different oxidizing agents, (b) Iron to oxygen molar ratio on the Fe-GAC in relation to the oxidizing agent used (The oxygen used in this calculation is the oxygen added to the GAC after reacting with different oxidizing agents).

weight percentage of different elements, we only used this ratio for a relative comparison. It can be seen from Fig. 2(b) that Fe/O molar ratio for $KMnO_4$ is higher than for other oxidizers, suggesting that oxidation is not the only prerequisite for loading of the iron on the GAC.

3.2.2. Role of manganese in iron loading

In an earlier study [9], the mechanism behind iron loading on GAC using $KMnO_4$ was proposed to be due to formation of manganese dioxide (MnO_2) on GAC. The hypothesis was that the $KMnO_4$ is reduced to manganese dioxide (MnO_2) on the GAC and that this MnO_2 plays a role in subsequent iron oxide formation. To check for the presence of MnO_2 on the oxidized GAC, the GAC with the highest loading of manganese was examined with XRD. However, there were no distinct peaks obtained that could be attributed to MnO_2 (Fig. S3 in Supporting information). This could be due to the amorphous nature of the GAC backbone. We checked the possible role of manganese in iron loading by mapping the manganese and iron distribution on GAC during the coating process (Fig. 3).

Fig. 3 shows that Fe distribution follows the Mn distribution on the GAC, which agrees with the hypothesis. We also found that the Fe and Mn distribution overlapped with the oxygen distribution, probably because the manganese and iron are expected to be present in their oxide forms. Another argument suggested in the earlier study [9] was that iron oxide formation occurs by displacing the manganese from the MnO_2. To confirm this hypothesis, the amount of manganese and iron on GAC-3 was monitored as a function of time during the reaction of the oxidized GAC in a ferric chloride solution (Fig. 4).

Fig. 4 shows a correlation between iron anchorage and release of manganese from the GAC. The molar ratio of iron anchored to manganese released was close to 1 under this experimental condition. Along with Figs. 2(b) and 3, 4 confirms the hypothesis that manganese plays a role in iron anchorage.

3.2.3. Characterization of Fe-GAC

To determine the type of iron oxide formed on the GAC, the Fe-GAC on GAC-3 was powdered and analyzed with X-ray Diffraction (XRD). However, we could not determine the type of iron oxide by XRD (data not shown), implying the iron oxide could be amorphous. Thus Mössbauer spectroscopy was used to determine the type of iron oxide (Fig. 5 and Table 1), with the advantage that even iron oxides with low crystallinity (amorphous) can be detected [27].

A earlier study [9] reports formation of magnetite (Fe_3O_4) when the GAC treated with $KMnO_4$ is reacted with a ferric chloride solution. Using Mössbauer spectroscopy, a doublet formation at 297 K with an isomer shift of 0.36 mm s^{-1} and a sextuplet formation at 86 K with a hyperfine field of 44 T was reported [9]. Our Mössbauer spectroscopy measurements (Fig. 5 and Table 1) show a doublet formation at 300 K with an isomer shift of 0.36 mm s^{-1} and sextuplet formation at 4.2 K having an average hyperfine field of 42.5 T (maximum value at ~45 T). It is possible that both studies have the same type of iron oxide. However, at 4.2 K the Fe^{3+} ion of magnetite has a hyperfine field around 50 T [28], whereas the hyperfine field we observed seems closer to ferrihydrite (around 46 T) [29]. Moreover, when the earlier study used 86 K, only 37% of the spectral contribution was magnetically split, and only 2% of the spectra were assigned an isomer shift that corresponds to Fe^{2+} ion [9]. In contrast, our measurements at 4.2 K resulted in 100% of the spectral contribution being magnetically split and all of it being assigned to Fe^{3+} ion. Thus our measurements are more suited to identify the type of iron oxide. Additionally, the broad magnetic field distribution of our sample (Fig. 5b) is a characteristic attributed to low crystallinity [30], which also points out that the Fe-GAC is most likely to have ferrihydrite. This agrees with our XRD observation of not being able to identify the iron oxide (Fig. S3 in Supporting information).

Reaction of $KMnO_4$ on activated carbon backbone to form MnO_2 has been reported multiple times [31–33]. However formation of

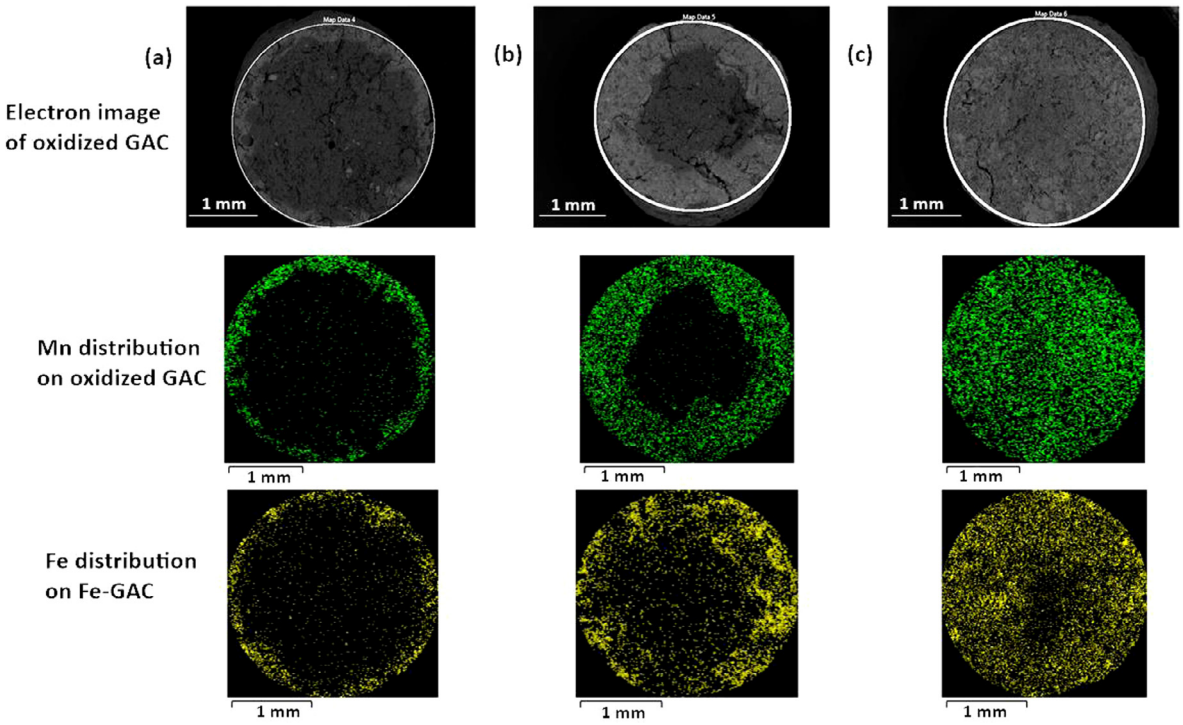

Fig. 3. Electron image and elemental distribution (using EDX) of GAC-1 cross sections. The GACs were contacted with $KMnO_4$ for the following durations: (a) 15 min (b) 2 h (c) 24 h. The contact time with $FeCl_3$ was 24 h in all cases.

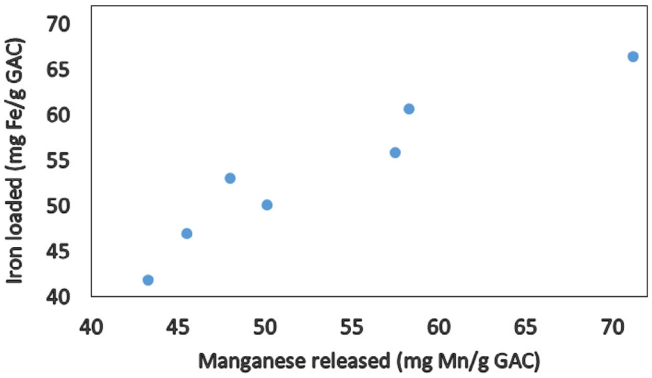

Fig. 4. Iron loaded as a function of manganese released from GAC-3.

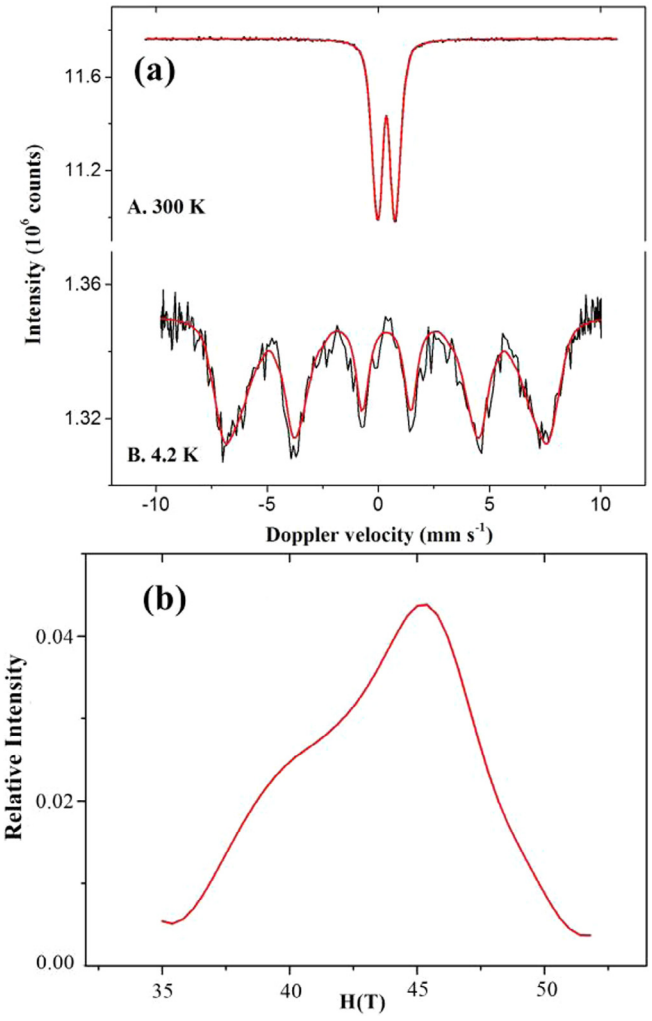

Fig. 5. (a) Mössbauer spectrum of Fe-GAC (from GAC-3) at 300 K and 4.2 K (b) Magnetic field distribution of the Fe-GAC.

magnetite on the $KMnO_4$ treated activated carbon backbone as per the earlier study [9] would require presence of ferrous ion (Fe^{2+}). But the ferric chloride solution used for loading iron consists of ferric ion (Fe^{3+}) and the conditions do not favor formation of Fe^{2+}. Therefore magnetite formation would not be possible and this is in line with our Mössbauer results. However, the exact mechanism of ferrihydrite formation has not been studied in our experiments and further study is needed to elaborate this mechanism. Our studies do establish that manganese loading is a prerequisite for iron loading on the activated carbon backbone.

To determine the size of the MnO_2 and ferrihydrite particles, the oxidized GAC and Fe-GAC formed using GAC-3 was observed with TEM (Fig. 6).

Fig. 6 shows the formation of needle like structures in oxidized GAC and Fe-GAC as compared to the GAC backbone. The size of these needle-like structures in the oxidized GAC as well as the Fe-GAC are above 10 nm. During the Mössbauer spectroscopy measurements a blocking temperature of around 25 K was measured for the ferrihydrite particles. As per literature, this indicates that the ferrihydrite particles in the Fe-GAC are around 4–5 nm [34]. The observed manganese particles are much bigger than the micropores and therefore it is unlikely that iron oxides are formed in the micropores in the subsequent treatment. Nevertheless during the coating process some of the smaller mesopores could be constricted to micropores because of the particles formed inside them. There might still be iron oxides found in such micropores.

3.3. Effect of PSD of different GACs

3.3.1. Manganese and iron loading on GACs with different PSD

Following the findings from the previous section, different GACs were treated with varying amount of $KMnO_4$ to find the optimum condition to maximize manganese loading (Fig. 7a). The oxidized GACs were subsequently reacted with ferric chloride to determine the highest possible iron loading on the Fe-GACs (Fig. 7b).

Fig. 7(a) shows that the manganese loading onto the GACs increased by using higher concentrations of $KMnO_4$. The overall manganese loading for the different GACs increased in the order: GAC-3 > GAC-2 > GAC-1 > GAC-4 > GAC-5. Fig. 7 (b) shows that the higher the manganese loading per GAC, the higher the iron loading on the GACs. This is in line with the hypothesis in Section 3.2 that manganese is required for iron anchorage on the GAC.

By comparing the results of Fig. 7(a) with Fig. 1, it can be seen that GACs with a higher portion of mesopores and macropores (or less micropores) had higher manganese loadings. Consequently the iron loading is higher in these GACs. Another observation is the ratio between the iron loading and manganese loading. The iron loaded seems to increase linearly at low manganese loadings. At higher manganese loadings, the amount of iron loaded is much lower than manganese loaded. This suggests that there is residual manganese loaded on the GAC that is not used to anchor iron.

3.3.2. P adsorption on adsorbents with different PSD

Adsorption isotherms are a vital tool for characterizing the performance of adsorbents. Adsorption tests were run for 4 days as this is already a long time considering practical applications.

Table 1
The Mössbauer fitted parameters of Fe-GAC (from GAC-3).

Sample	T (K)	IS (mm s^{-1})	QS (mm s^{-1})	Hyperfine field (T)	Γ (mm s^{-1})	Phase	Spectral contribution (%)
Fe/GAC	300	0.36	0.89	–	0.30	Fe^{3+}	100
Fe/GAC	4.2	0.37	0	42.5*	0.57	Fe^{3+}	100

Experimental uncertainties: Isomer shift: I.S. ± 0.01 mm s^{-1}; Quadrupole splitting: Q.S. ± 0.01 mm s^{-1}; Line width: Γ ± 0.01 mm s^{-1}; Hyperfine field: ±0.1 T; Spectral contribution: ±3%. *Average magnetic field.

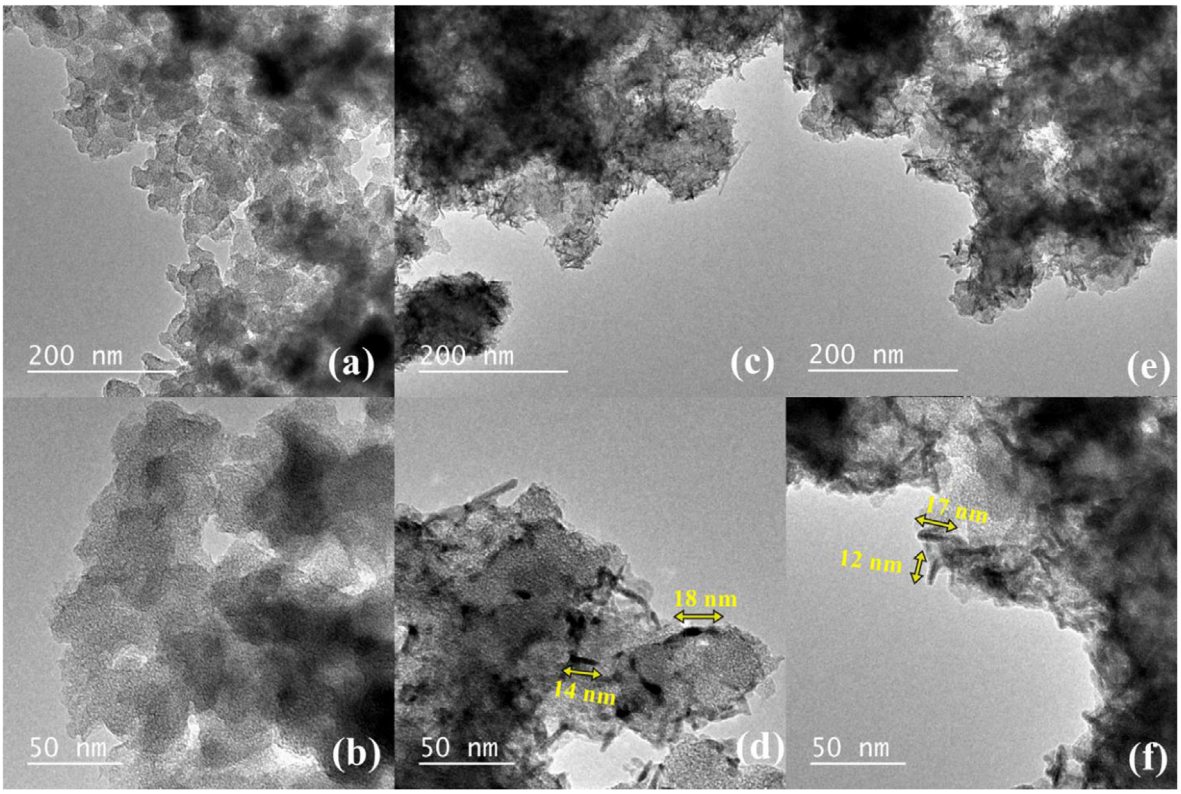

Fig. 6. TEM images of (a) GAC-3, (b) GAC-3 at higher magnification (c) oxidized GAC-3 (d) oxidized GAC-3 at higher magnification (e) Fe-GAC-3 (f) Fe-GAC-3 at higher magnification.

Adsorption kinetics (Fig. S2 in Supporting information) were fitted with pseudo second order model to show that after 4 days we were within 5% of reaching equilibrium in all cases (Table S6 in Supporting info). GAC-4 and GAC-5 were not included for P adsorption isotherms since they showed very low iron loading and preliminary experiments showed they could not adsorb P.

Fig. 8 shows the adsorption capacities for the different Fe-GACs as a function of final concentration of phosphate. Phosphate adsorption on iron oxides happens via ligand exchange reaction, in other words via chemisorption [35]. Therefore, the Langmuir isotherm model, which assumes chemisorption at the adsorption mechanism [36], was used to fit the experimental adsorption data.

The Langmuir expression is:

$$q_e = \frac{q_m K_L C_e}{(1 + K_L C_e)} \quad (2)$$

where,

q_m = Maximum adsorption capacity (mg P/g),
q_e = Adsorption capacity at equilibrium (mg P/g),
C_e = Concentration at equilibrium (mg P/L),
K_L = Equilibrium constant for the Langmuir adsorption (L/mg P).

Table 2 compares the Langmuir parameters of the different adsorbents in relation to their surface area, iron anchorage and residual manganese content. The residual manganese is the remaining manganese after the iron loading process. To determine if the manganese also plays a role in phosphate adsorption, oxidized GAC-3 with a very high manganese loading (200 mg Mn/g) but before iron anchorage was tested. It's adsorption capacity at the maximum phosphate concentration used in isotherms was 3.5 mg P/g. This is about 3 times lower than adsorption capacity of Fe-GACs. Therefore, even though the residual manganese in the Fe-GACs could contribute to phosphate adsorption, the iron contributes for a majority of the phosphate adsorption. Table 2 shows that the constant K_L, which correlates with adsorption at lower phosphate concentration correlates rather to the iron content of the adsorbents than to the manganese content.

For application of adsorption as a polishing step in municipal wastewater treatment, we are most interested in examining the adsorption at low phosphate concentrations (<10 mg P/L). Therefore the initial slopes of the adsorption isotherm curves are most relevant. Fig. 8 shows that the different GACs vary in their P adsorption capacity especially at lower concentration, as indicated by the different slopes in the initial part of the curves. To quantify the difference in adsorption of GACs at lower concentrations, we make use of the Langmuir parameters. We define the term adsorption affinity as the constant that relates adsorption capacity to very low adsorbate concentrations. This term is determined by the slope of the Langmuir adsorption curve as the concentration of phosphate tends to zero. As $C_e \rightarrow 0$ (and provided K_L is finite) in the Langmuir equation, the equation becomes:

$$q_e = q_m K_L C_e \quad (3)$$

The term, $q_m K_L$, represents the slope of the initial part of the isotherm curve, and denotes the adsorption affinity. The above equation means that at very low concentrations, the equilibrium adsorption capacity depends on the total number of active sites rather than the number of unoccupied active sites.

Fig. 9 shows that the adsorption affinity correlated with the porous area of the adsorbents if we assume a cut off pore size of 2 nm. However, if we assume a cut off pore size of 3 nm, we get a correlation with zero intercept which means a completely proportional relation. A majority of this porous area is in the mesopores as compared to the macropores (see Tables S4 and S5), which highlights the importance of mesopores. For GAC-3, the mesoporous area increases after iron loading. This is possibly due to the high fraction of macropores in GAC-3, which gets constricted

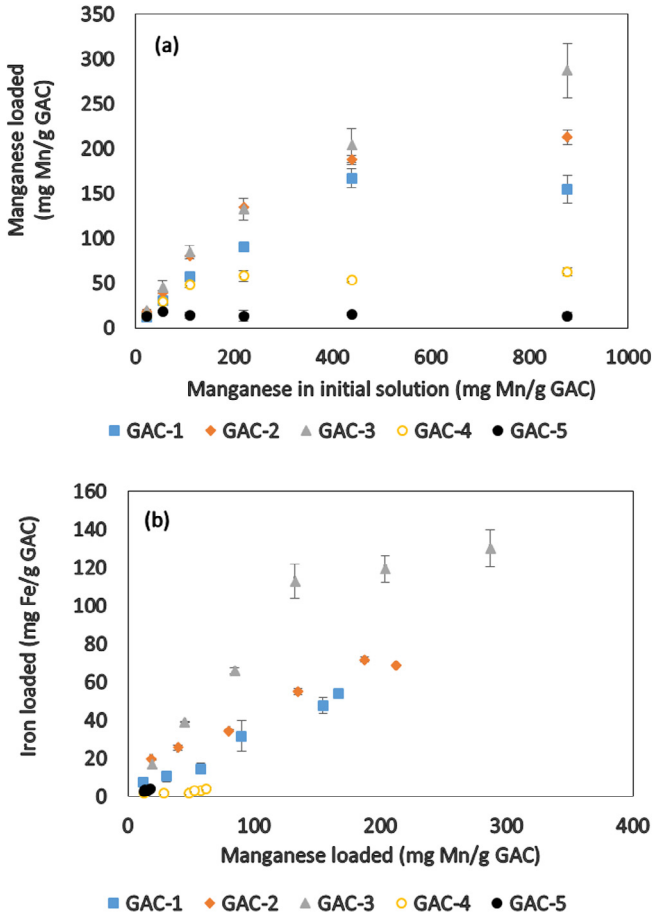

Fig. 7. (a) Manganese loading onto different GACs as a function of available manganese, (b) Iron loading onto different GACs as a function of manganese loaded.

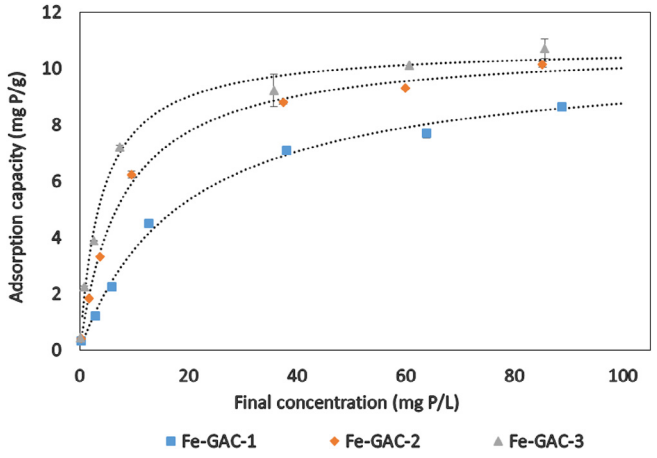

Fig. 8. P adsorption isotherm (at 22 °C) for the different Fe-GACs. The dashed lines represent the Langmuir fit for each adsorbent.

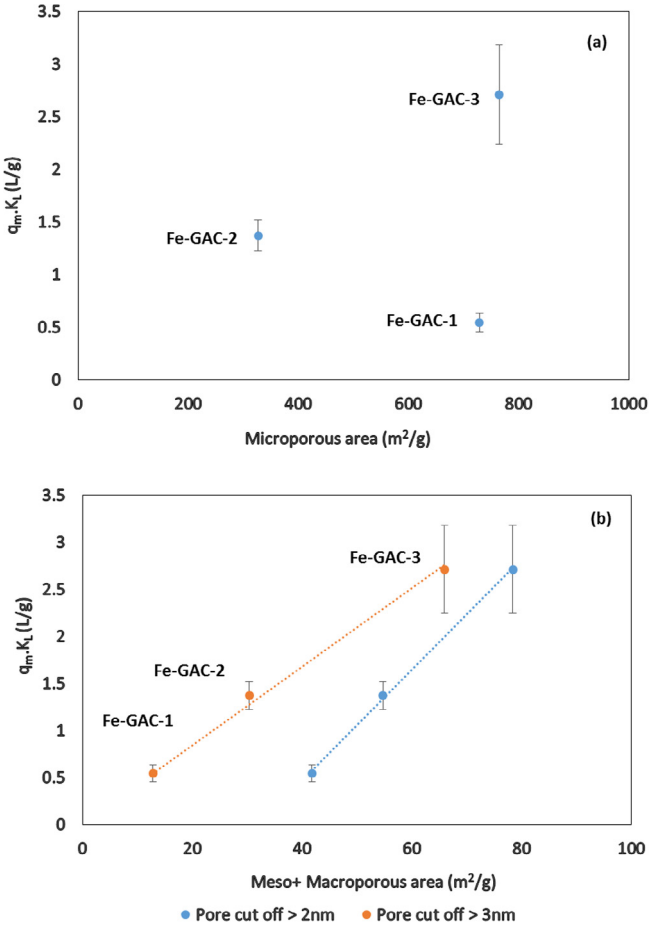

Fig. 9. Correlation of adsorption affinity of different Fe-GACs to (a) microporous area (b) meso + macroporous area (Pore cut off >3 nm, correlation coefficient: 0.995) The NLDFT model was used for estimating the microporous and mesoporous area. The BJH model was used for estimating the macroporous area.

to mesopores during the coating process. One explanation for the microporous area not contributing to P adsorption affinity could be the iron coating process. Fig. 6 indicates that the MnO_2 particles are much bigger than the micropores and hence iron oxides would also not be formed in the micropores. Thus the only micropores in the Fe-GAC that contribute to the adsorption would be those that were formed as a result of pore blocking of mesopores. Hence a majority of the micropores would not be contributing to P adsorption. Additionally the diffusion of phosphate ions in the micropores could be difficult. Phosphate ions have a diameter of about 0.48 nm [37]. Thus the adsorbate molecule is in a similar order of magnitude to the micropores and this could lead to hindered diffusion in such pores [38]. The decrease in diffusion would especially be significant at low concentrations of phosphate where the driving force for diffusion is less. Thus the adsorption affinity would be largely related to mesopores and macropores. But because the surface area is significantly higher for the mesopores compared to the macropores, the mesopores will be the main contributing factor to adsorption.

Table 2
Langmuir model parameters along with BET surface area, iron and residual manganese content of the adsorbents.

Sample	BET surface area (m^2/g)	Fe anchored (mg Fe/g)	Residual manganese (mg Mn/g)	q_m (mg P/g adsorbent)	K_L (L/mg P)
Fe-GAC-1	920 ± 5	48 ± 4	76 ± 21	10.4 ± 0.4	0.05 ± 0.01
Fe-GAC-2	441 ± 30	69 ± 0.3	147 ± 8	10.8 ± 0.2	0.13 ± 0.01
Fe-GAC-3	794 ± 1	113 ± 9	31 ± 18	10.8 ± 0.3	0.25 ± 0.04

4. Conclusion

High phosphate adsorption capacities can be achieved by coating high surface area backbones (like granular activated carbon) with iron oxide nanoparticles. This study shows that ferrihydrite nanoparticles can be coated on the GAC backbone using $KMnO_4$. Manganese loading on the GAC as an intermediate step is important for this process. However this study shows that the manganese oxide particles that serve as a precursor for the ferrihydrite formation have needle like structures with a length of more than 10 nm. This result suggests that only a fraction of the total pore area in the GAC is actually coated with manganese oxide and iron oxide particles because the pore area in GAC is dominated by micropores with a pore size smaller than 2 nm. Testing of GACs with different PSD showed that the adsorption at low P concentrations correlates well with the mesoporous area of the adsorbents.

This result suggests that the applied coating method is best suited for backbones with predominantly mesoporous pore size distributions. Nevertheless the application on GAC's with predominantly micropores could still be of interest if these micropores can serve another function, for instance to adsorb micropollutants. Combined removal of phosphate (in the mesopores) and micropollutants (in the mesopores) could be an interesting prospect for polishing of sewage treatment effluents in light of stringent demands and limits to effluent quality.

Acknowledgements

This work was performed in the TTIW-cooperation framework of Wetsus, European Centre Of Excellence For Sustainable Water Technology (www.wetsus.nl). Wetsus is funded by the Dutch Ministry of Economic Affairs, the European Union Regional Development Fund, the Province of Fryslân, the City of Leeuwarden and the EZ/Kompas program of the "Samenwerkingsverband Noord-Nederland". We thank the participants of the research theme "Phosphate Recovery" for their financial support and helpful discussions. We thank Maarten Biesheuvel and Bert Hamelers from Wetsus for their useful feedback.

Appendix A. Supplementary data

Supplementary data associated with this article can be found, in the online version, at http://dx.doi.org/10.1016/j.cej.2017.05.147.

References

[1] D. Cordell, J.-O. Drangert, S. White, The story of phosphorus: global food security and food for thought, Global Environ. Change 19 (2009) 292–305.
[2] L. Reijnders, Phosphorus resources, their depletion and conservation, a review, Resour. Conserv. Recycl. 93 (2014) 32–49.
[3] H.P. Jarvie, C. Neal, P.J.A. Withers, Sewage-effluent phosphorus: a greater risk to river eutrophication than agricultural phosphorus?, Sci Total Environ. 360 (2006) 246–253.
[4] P. Loganathan, S. Vigneswaran, J. Kandasamy, N.S. Bolan, Removal and recovery of phosphate from water using sorption, Crit. Rev. Environ. Sci. Technol. 44 (2014) 847–907.
[5] L.M. Blaney, S. Cinar, A.K. SenGupta, Hybrid anion exchanger for trace phosphate removal from water and wastewater, Water Res. 41 (2007) 1603–1613.
[6] P. Wilfert, P.S. Kumar, L. Korving, G.-J. Witkamp, M.C.M. van Loosdrecht, The relevance of phosphorus and iron chemistry to the recovery of phosphorus from wastewater: a review, Environ. Sci. Technol. 49 (2015) 9400–9414.
[7] J. Lalley, C. Han, X. Li, D.D. Dionysiou, M.N. Nadagouda, Phosphate adsorption using modified iron oxide-based sorbents in lake water: kinetics, equilibrium, and column tests, Chem. Eng. J. 284 (2016) 1386–1396.
[8] W. Huang, Y. Zhu, J. Tang, X. Yu, X. Wang, D. Li, Y. Zhang, Lanthanum-doped ordered mesoporous hollow silica spheres as novel adsorbents for efficient phosphate removal, J. Mater. Chem. A 2 (2014) 8839–8848.
[9] A. Zach-Maor, R. Semiat, H. Shemer, Synthesis, performance, and modeling of immobilized nano-sized magnetite layer for phosphate removal, J. Colloid Interface Sci. 357 (2011) 440–446.
[10] F. Çeçen, Ö. Aktaş, Removal of NOM, Nutrients, and Micropollutants in BAC Filtration, Activated Carbon for Water and Wastewater Treatment, Wiley-VCH Verlag GmbH & Co KGaA, 2011, pp. 265–318.
[11] F.J. García-Mateos, R. Ruiz-Rosas, M.D. Marqués, L.M. Cotoruelo, J. Rodríguez-Mirasol, T. Cordero, Removal of paracetamol on biomass-derived activated carbon: modeling the fixed bed breakthrough curves using batch adsorption experiments, Chem. Eng. J. 279 (2015) 18–30.
[12] R.R. Gil, B. Ruiz, M.S. Lozano, M.J. Martín, E. Fuente, VOCs removal by adsorption onto activated carbons from biocollagenic wastes of vegetable tanning, Chem. Eng. J. 245 (2014) 80–88.
[13] J. Rivera-Utrilla, M. Sánchez-Polo, V. Gómez-Serrano, P.M. Álvarez, M.C.M. Alvim-Ferraz, J.M. Dias, Activated carbon modifications to enhance its water treatment applications. An overview, J. Hazard. Mater. 187 (2011) 1–23.
[14] L. Zhang, L. Wan, N. Chang, J. Liu, C. Duan, Q. Zhou, X. Li, X. Wang, Removal of phosphate from water by activated carbon fiber loaded with lanthanum oxide, J. Hazard. Mater. 190 (2011) 848–855.
[15] J. Liu, Q. Zhou, J. Chen, L. Zhang, N. Chang, Phosphate adsorption on hydroxyl–iron–lanthanum doped activated carbon fiber, Chem. Eng. J. 215–216 (2013) 859–867.
[16] Q. Zhou, X. Wang, J. Liu, L. Zhang, Phosphorus removal from wastewater using nano-particulates of hydrated ferric oxide doped activated carbon fiber prepared by Sol-Gel method, Chem. Eng. J. 200–202 (2012) 619–626.
[17] Z. Klencsár, Mössbauer spectrum analysis by Evolution Algorithm, Nucl. Instrum. Methods Phys. Res. Sect. B 129 (1997) 527–533.
[18] K.J. Keesman, System Identification: An Introduction, Springer Science & Business Media, 2011.
[19] K.S.W. Sing, D.H. Everett, R.A.W. Haul, L. Moscou, R.A Pierotti, J. Rouquerol, T. Siemieniewska, Reporting Physisorption Data for Gas/Solid Systems, Handbook of Heterogeneous Catalysis, Wiley-VCH Verlag GmbH & Co. KGaA, 2008.
[20] J. Rouquerol, D. Avnir, C. Fairbridge, D. Everett, J. Haynes, N. Pernicone, J. Ramsay, K. Sing, K. Unger, Recommendations for the characterization of porous solids (technical report), Pure Appl. Chem. 66 (1994) 1739–1758.
[21] K. Sing, The use of nitrogen adsorption for the characterisation of porous materials, Colloids Surf., A 187–188 (2001) 3–9.
[22] E.P. Barrett, L.G. Joyner, P.P. Halenda, The determination of pore volume and area distributions in porous substances. I. Computations from nitrogen isotherms, J. Am. Chem. Soc. 73 (1951) 373–380.
[23] R.F. Cracknell, K.E. Gubbins, M. Maddox, D. Nicholson, Modeling fluid behavior in well-characterized porous materials, Acc. Chem. Res. 28 (1995) 281–288.
[24] T. Matthias, Physical Adsorption Characterization of Ordered and Amorphous Mesoporous Materials, Nanoporous Materials: Science and Engineering, Published By Imperial College Press and Distributed By World Scientific Publishing Co., 2004, pp. 317–364.
[25] J. Landers, G.Y. Gor, A.V. Neimark, Density functional theory methods for characterization of porous materials, Colloids Surf., A 437 (2013) 3–32.
[26] Z. Wang, E. Nie, J. Li, M. Yang, Y. Zhao, X. Luo, Z. Zheng, Equilibrium and kinetics of adsorption of phosphate onto iron-doped activated carbon, Environ. Sci. Pollut. Res. 19 (2012) 2908–2917.
[27] R.M. Cornell, U. Schwertmann, Characterization, The Iron Oxides, Wiley-VCH Verlag GmbH & Co KGaA, 2004, pp. 139–183.
[28] L. Sang Won, S.J. Kim, S. In-Bo, B. Seongtae, K. Chul Sung, Mössbauer studies of nano-size controlled iron oxide for biomedical applications, IEEE Trans. Magn. 41 (2005) 4114–4116.
[29] E. Murad, The Mössbauer spectrum of "well"-crystallized ferrihydrite, J. Magn. Magn. Mater. 74 (1988) 153–157.
[30] E. Murad, Properties and behavior of iron oxides as determined by mössbauer spectroscopy, in: J.W. Stucki, B.A. Goodman, U. Schwertmann (Eds.), Iron in Soils and Clay Minerals, Springer, Netherlands, Dordrecht, 1988, pp. 309–350.
[31] B. Liu, A.M. Li, M.F. Xia, Z.L. Zhu, Preparation of manganese oxide supported on activated carbon and its application in catalytic ozonation of 4-chlorophenol, Trans. Tech. Publ. Adv. Mater. Res. (2012) 2285–2288.
[32] D. Deng, B.-S. Kim, M. Gopiraman, I.S. Kim, Needle-like MnO_2/activated carbon nanocomposites derived from human hair as versatile electrode materials for supercapacitors, RSC Adv. 5 (2015) 81492–81498.
[33] H. Song, X. Li, Y. Zhang, H. Wang, H. Li, J. Huang, A nanocomposite of needle-like MnO_2 nanowires arrays sandwiched between graphene nanosheets for supercapacitors, Ceram. Int. 40 (2014) 1251–1255.
[34] E. Murad, J. Cashion, Iron Oxides Mössbauer Spectroscopy of Environmental Materials and Their Industrial Utilization, Springer, US, Boston, MA, 2004, pp. 159–188.
[35] R.M. Cornell, U. Schwertmann, Adsorption of Ions and Molecules, The Iron Oxides, Wiley-VCH Verlag GmbH & Co KGaA, 2004, pp. 253–296.
[36] I. Langmuir, The adsorption of gases on plane surfaces of glass, mica and platinum, J. Am. Chem. Soc. 40 (1918) 1361–1403.
[37] D.S. Tawfik, R.E. Viola, Arsenate replacing phosphate – alternative life chemistries and ion promiscuity, Biochemistry 50 (2011) 1128–1134.
[38] R.E. Beck, J.S. Schultz, Hindrance of solute diffusion within membranes as measured with microporous membranes of known pore geometry, Biochim. Biophys. Acta 255 (1972) 273–303.